Quantum Emitters Near a Metal Nanoparticle: Strong Coupling and Quenching

A. Delga, J. Feist, J. Bravo-Abad, and F. J. Garcia-Vidal

Departamento de Física Teórica de la Materia Condensada and Condensed Matter Physics Center (IFIMAC),
Universidad Autónoma de Madrid, E-28049 Madrid, Spain

We investigate the interplay between quenching and strong coupling in systems that include a collection of quantum emitters interacting with a metal nanoparticle. By using detailed numerical simulations and analytical modeling, we demonstrate that quantum emitters can exhibit strong coupling with the particle dipole resonance at distances at which the quenching to nonradiative channels is expected to dominate the dynamics. These results can be accounted for in terms of the pseudomode character of the higher multipole modes of the nanoparticle and the corresponding reduction of the induced loss rate. These findings expand the current understanding of light-matter interaction in plasmonic systems and could contribute to the development of novel quantum plasmonic platforms.

Metal particles are able to support electromagnetic (EM) resonances, usually called localized surface plasmons (LSPs). For particles of spherical shape, these EM modes are characterized by their angular momentum, l. When the dimension of the particle is much smaller than the plasmon wavelength (of the order of hundreds of nm), its optical response is dominated by the dipolar mode, $l = 1$. However, when a quantum emitter (QE) is placed in close proximity to the particle, the nonradiative EM modes ($l > 1$) are the main channel for decay and the QE fluorescence is strongly quenched [1–4]. Quenching is a hurdle on the road towards efficient optical antennas [5], spasers [6–8], or subwavelength optical circuits [9].

Similarly, the large effective decay rates induced by quenching are expected to suppress strong coupling, which is reached when the energy exchange rate between the QE and EM modes becomes faster than the decay rates. In recent years, there has been renewed interest in the emergence of strong coupling between QEs and surface plasmons supported by different metallic structures. Although most studies have focused on planar metal surfaces [10–14], some theoretical works have been devoted to analyzing the interaction between a single QE and a metal nanoparticle [15–19] or a dimer [20]. For an ensemble of QEs, collective strong coupling to LSPs has been observed experimentally [21–23], and LSP-mediated superradiance has been predicted theoretically [24].

In this Letter, we present an in-depth study of the interplay between quenching and strong coupling of a single QE or a collection of QEs interacting with a metal nanoparticle. This fundamental analysis is based on a macroscopic QED numerical framework that can treat an arbitrary number of QEs coupled to plasmonic systems. As shown below, for a single QE placed near a metal nanoparticle, strong coupling only appears at very short distances and the associated reversible exchange of energy occurs between the QE and a

pseudomode consisting of the nonradiative multipole resonances. However, for an ensemble of QEs, collective strong coupling of the QEs with the dipole mode of the nanoparticle emerges for a broad range of distances, even close to the surface where quenching is expected. Importantly, the results of our numerical formalism are mapped into a three-level Hamiltonian that allows us to find analytical formulas for the relevant physical magnitudes.

The model system under study (Fig. 1) is a metal nanoparticle of radius a, whose dielectric response is characterized by a Drude formula, $\epsilon_m(\omega) = \epsilon_\infty - \omega_p^2/[\omega(\omega + i\gamma_p)]$. The nanoparticle is embedded in a nondispersive, lossless dielectric medium with ϵ_d, which also hosts the QEs. For simplicity, we use a homogeneous shell of N radially oriented QEs placed at a distance h from the surface of the spherical particle. The generalization of our numerical results to other configurations of the QEs is straightforward. The QEs are modeled as pointlike two-level systems with transition frequency ω_0, internal nonradiative decay rate
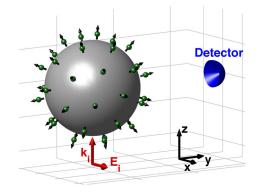

FIG. 1 (color online).   Schematics of the system under study: a metal nanoparticle is surrounded by a collection of quantum emitters that are homogeneously distributed in a spherical shell and whose dipole orientations are radial.

γ_{QE}, and transition dipole moment $\vec{\mu}$. The system is excited by an x-polarized plane wave impinging along the z direction, and the output signal is collected by a detector placed in the far field region.

We first briefly revisit the case of a single QE (located at $\vec{r}$) interacting with a metal nanoparticle. As reported in Ref. [25], the dynamics of this system is determined by the so-called spectral density, $J(\omega) = \omega^2/(\pi\hbar\epsilon_0 c^2)\vec{\mu} \cdot \Im m \mathbf{G}(\vec{r}, \omega) \cdot \vec{\mu}$. Analytical insight can be obtained in the quasistatic limit ($a, h \ll \lambda$), where the radial term of the Green's function can be written as

$$\mathbf{G}^{rr}(r, \omega) = \mathbf{G}_0^{rr} + \frac{c^2}{4\pi\omega^2\epsilon_d a^3} \sum_{l=1}^{\infty} \frac{(l+1)^2}{(1+\zeta)^{2l+4}} \frac{\epsilon_m - \epsilon_d}{\epsilon_m + \frac{l+1}{l}\epsilon_d},$$

(1)

where $r = h + a$ and $\zeta = h/a$. The homogeneous contribution to the total Green's function, $\mathbf{G}_0^{rr} = \omega\sqrt{\epsilon_d}/(6\pi c)$, is negligible for the spatial regions of interest. At large distances ($h > 0.7a$), the contribution to J coming from the metal nanoparticle, $J_{NP}(\omega)$ [associated with the sum in the right-hand side of Eq. (1)], is dominated by the dipole mode which appears at $\omega_1 = 3.01$ eV ($l = 1$, $\epsilon_m = -2\epsilon_d$), see Fig. 2(a). For shorter distances, however, the high-order multipole modes converging towards $\omega_\infty = 3.45$ eV
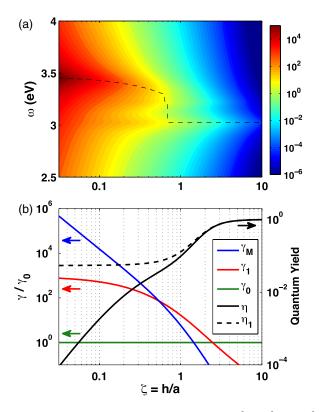

(a)

(b)

FIG. 2 (color online).   (a) J_{NP} in units of $\mu^2/(4\pi^2\epsilon_d\epsilon_0\hbar a^3)$ as a function of ζ and ω. The dashed black line is a guide for the eye that follows the maximum of J_{NP}. (b) Normalized decay rates, γ_1 and γ_M, and quantum yields, η and η_1, as a function of ζ for $\omega_0 = 2.5$ eV.

($l \to \infty$, $\epsilon_m = -\epsilon_d$) prevail. For metal spheres of subwavelength size, the dipole mode is by far the most radiative EM mode although its nonradiative Ohmic losses are significant. In contrast, the higher multipole modes ($l > 1$) can be safely considered as purely nonradiative.

Fluorescence quenching only applies in the weak coupling regime. In this limit, the EM modes are treated as a quasicontinuum, i.e., a Markovian loss channel, and the QE decay rate is given by $\Gamma = 2\pi J(\omega_0)$. The quenching region is entered when the QE quantum yield (η), defined as the ratio between the radiative decay rate and total Γ, is close to zero. The multipolar expansion of $\mathbf{G}^{rr}$ also allows us to distinguish between the QE decay rate into the dipole mode (γ_1) and the contribution of all higher (nonradiative) multipoles (γ_M). In Fig. 2(b), we render these two magnitudes (γ_1 and γ_M) evaluated at $\omega_0 = 2.5$ eV as a function of ζ. For these calculations and for those shown in the rest of the Letter, we have used $a = 7$ nm and $\epsilon_d = 2.13$, which correspond to the experiment reported in Ref. [7], and the full Green's function as given in Ref. [26]. The nanoparticle is assumed to be made of silver, with Drude parameters $\epsilon_\infty = 4.6$, $\omega_p = 9$ eV, and $\gamma_p = 0.1$ eV taken from tables [27]. The two decay rates (γ_1 and γ_M) are normalized to the radiative QE decay rate in vacuum, $\gamma_0 = \mu^2\omega_0^3/(3\pi\epsilon_0\hbar c^3)$. Also in Fig. 2(b) we plot the evolution of η and η_1 (quantum yield calculated by considering only the dipole mode in the nanoparticle) as a function of ζ. It is clear that the huge decrease of η observed at very short distances is due to the prevalence of the higher multipole modes in this limit ($\gamma_M \gg \gamma_1$).

As stated above, the concept of quenching breaks down when strong coupling between the QE and the EM modes of the nanoparticle emerges. In this regime, the higher multipole modes can then no longer be treated as a quasicontinuum, and a description as a pseudomode with loss rate γ_p becomes more appropriate. In order to analyze the strong coupling case, we use a macroscopic QED formalism [17,28,29] that is suited to describe lossy media. It relies on the diagonalization of a Hamiltonian that includes the ensemble of QEs, the EM modes of the metal nanoparticle including their inherent losses, and the light-matter coupling by means of a dipolar interaction,

$$\mathcal{H} = \int d^3\mathbf{r} \int_0^\infty d\omega\hbar\omega\hat{\mathbf{f}}^\dagger(\mathbf{r}, \omega)\hat{\mathbf{f}}(\mathbf{r}, \omega) + \sum_{n=1}^{N} \frac{\hbar\Omega_n}{2}\hat{\sigma}_n^z$$

$$- \sum_{n=1}^{N} [\hat{\sigma}_n^+ + \hat{\sigma}_n^-]\vec{\mu}_n \cdot (\hat{\mathbf{F}}^{(+)}(\mathbf{r}) + \hat{\mathbf{F}}^{(-)}(\mathbf{r})),$$

(2)

where $\Omega_n = \omega_0 - i\gamma_{QE}/2$ and the resulting polaritonic operators $\hat{\mathbf{f}}(\mathbf{r}, \omega)$ represent the elementary excitations of the light-matter system, including LSPs. The QEs are described in terms of the fermionic operators $\hat{\sigma}_n$. We stress that no rotating wave approximation is made in the coupling term, making this formalism suited to study

ultrastrong coupling regimes as well. The E-field operators
are given by

$$\hat{\mathbf{F}}^{(+)}(\mathbf{r}) = i\sqrt{\frac{\hbar}{\pi\epsilon_0}} \int_0^\infty d\omega \frac{\omega^2}{c^2}$$

$$\times \int d^3\mathbf{r}' \sqrt{\epsilon_m^I(\mathbf{r}',\omega)} \mathbf{G}(\mathbf{r},\mathbf{r}',\omega)\hat{\mathbf{f}}(\mathbf{r}',\omega), \quad (3)$$

where ϵ_m^I is the imaginary part of ϵ_m and $\mathbf{G}(\mathbf{r},\mathbf{r}',\omega)$ is the
frequency-dependent EM Green's function that connects
points $\mathbf{r}$ and $\mathbf{r}'$ in space. Direct dipole-dipole interactions are
naturally included in the total Green's function. By bosoniz-
ing the fermionic operators in the Heisenberg equations of
motion and by tracing them out, we get a Lippman-
Schwinger equation for $\hat{\mathbf{F}}$, where the QEs appear as point
scatterers and quantum source operators. In the end, the E-
field operators are obtained by means of a multiple-scattering
problem, which is solved by generalizing a procedure
previously introduced for nondispersive, lossless media [30].

To quantify strong coupling in our system, we rely on a
physical magnitude that has experimental relevance, the
light spectrum measured at the detector position, $S(\mathbf{R},\omega)$.
In typical experimental setups, QEs are incoherently
pumped at high energies. To mimic this setup, we calculate
the light spectra for an initial excitation of each QE
separately and sum them incoherently, weighted by the
incident field intensities at the emitter positions. We keep
the illumination power constant when varying the number
of QEs. The expression for the light spectrum with the
initially excited n_0th QE is given by

$$S_{n_0}(\mathbf{R},\omega) = \sum_n \left| \frac{\omega^2}{\epsilon_0 c^2} \mathbf{G}^{(N)}(\mathbf{R},\mathbf{r_n},\omega)\cdot\vec{\mu}_n \right|^2$$

$$\times \left(\frac{\delta_{n,n_0}}{|\omega - \Omega_n|^2} + \frac{1-\delta_{n,n_0}}{|\omega + \Omega_n|^2} + \frac{\delta_{n,n_0}}{|\omega + \Omega_n|^2} \right), \quad (4)$$

where $\mathbf{G}^{(N)}(\mathbf{R},\mathbf{r_n},\omega)$ is the N-scattering dressed Green's
function describing the full propagation from the nth QE to
the detector. This result is analytical and valid in both weak
and strong coupling regimes. More details of our numerical
framework can be found in the Supplemental Material [31].

In Fig. 3 we consider a layer of N QEs placed at
$h = 1$ nm. For these calculations we have taken $\mu = 0.19\ e \cdot$
nm and $\gamma_{QE} = 15$ meV, which are typical values for
organic molecules [12]. The gap in the light spectrum
close to ω_∞ for $N = 1$ clearly shows that a single QE can
indeed reach strong coupling with the nonradiative LSP
modes of the metal nanoparticle. This strong coupling
regime for a single QE has previously been predicted for
the case of a metal nanoparticle [15,17] and also for a
planar metal surface [14]. However, as the number of QEs
increases, far field signatures of strong coupling disappear
at $\omega_0 \approx \omega_\infty$ while cooperative strong coupling with the
radiative dipole mode builds up and a gap opens at
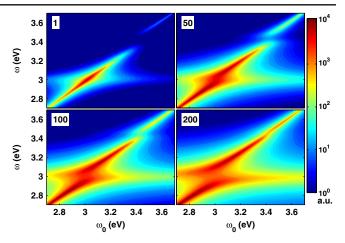$\omega_0 = \omega_1$, which increases with N. This behavior is one

FIG. 3 (color online). Contour plots of the light spectra
measured at the detector position, which is placed 1 μm away
from the center of the nanoparticle along the y axis. This
magnitude is rendered for different values of the number of
QEs homogeneously distributed in a shell at $h = 1$ nm.

of the main results of this Letter: collective strong coupling
with the dipole mode can emerge even at very short
distances to the surface, where the interaction between
the QEs and the metal nanoparticle is expected to be
dictated by the nonradiative modes. As we will show below,
the higher multipole modes again do not behave as a
featureless continuum, but as a far-detuned pseudomode
with decay rate γ_p that does not efficiently channel
excitation out of the emitter. It is also worth noticing that
the total detector signal (light spectrum integrated over
frequency) increases by a factor of 420 when comparing the
single-QE case at $\omega_0 \approx \omega_\infty$ with the case of 200 QEs with
transition frequency $\omega_0 = \omega_1$.

We next investigate the apparent closing of the gap for
$\omega_0 \approx \omega_\infty$ as N is increased. In Fig. 4(a) we show the
evolution of the light spectrum as a function of N. It is clear
that one single peak overcomes the signature of the
individual strong coupling in the far-field spectrum. To
gain more insight into this effect, we show in Fig. 4(b) the
near-field polarization spectra, $P_n(\omega) = \langle\hat{\sigma}_n^+(-\omega)\hat{\sigma}_n^-(\omega)\rangle$,
for the same cases analyzed in Fig. 4(a). The polarization
spectrum indeed displays the two peaks corresponding to
the strong coupling between a single QE and the non-
radiative modes. Notice that the frequency splitting
between these hybrid modes does not increase with N.
Additionally, a second feature emerges [marked by arrows
in Fig. 4(b)], which is the signature of the strongly coupled
state formed between the ensemble of QEs and the highly
detuned ($\delta = 0.4$ eV) dipole mode of the nanoparticle.
This is the only feature observed in the far field, implying
that propagation to the detector acts as a filter. The field
distribution on the surface of the metal nanoparticle, plotted
for $\omega_0 \approx \omega_\infty$ in Fig. 4(c), is illustrative of the interplay
between local and collective effects. The spots underneath
each QE correspond to pseudomodes formed from
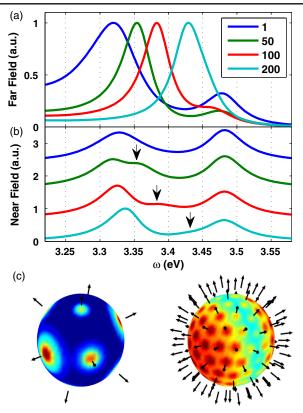localized superpositions of multipole modes interacting

FIG. 4 (color online).   (a) Light spectra at the detector position for $\omega_0 \approx \omega_\infty$ and $h = 1$ nm. (b) Corresponding polarization spectra for the same cases analyzed in panel (a). (c) Contour plots of the near-field spectrum evaluated at the surface of the metal nanoparticle for $N = 10$ and $N = 100$. The color scales are identical in both panels [blue (red) corresponds to minimum (maximum) of the E field].

separately with each emitter. They do not disappear with N—instead, the dipole mode encompassing the whole nanoparticle clearly emerges in the background when N is increased. These characteristics of the field distribution illustrate why coupling to the radiative dipole mode is cooperative, while interaction with the pseudomode is noncollective and spatially localized.

Finally, we develop an analytical model that provides further physical insight into the numerical results. Based on the multipolar expansion of the Green's function as given in Eq. (1), $J_{NP}(\omega)$ can be written as a sum of Lorentzians, similar to the case of a planar metal surface [14]:

$$J_{NP}(\omega) \approx \sum_{l=1}^{\infty} \frac{g_l^2}{\pi} \frac{\gamma_p/2}{(\omega - \omega_l)^2 + (\gamma_p/2)^2}, \quad (5)$$

where $\omega_l = \omega_p / \sqrt{\epsilon_\infty + (1 + 1/l)\epsilon_d}$ is the frequency of the LSP resonance with angular momentum l. From this expansion, the coupling g_l between the QE and LSP with angular momentum l can be identified as

$$g_l^2 = \frac{\mu^2 \omega_p}{4\pi\epsilon_0 \hbar a^3} \left(\frac{\omega_l}{\omega_p}\right)^3 \frac{(l+1)^2}{(1+\zeta)^{2l+4}} \left(1 + \frac{1}{2l}\right). \quad (6)$$

A very good approximation to our numerical results can then be obtained by a three-level Hamiltonian involving the following modes: (i) a collective excitation of the ensemble of QEs, (ii) the radiative dipole mode of the nanoparticle, and (iii) a pseudomode formed by all the nonradiative modes of the metal nanoparticle. The associated three-level Hamiltonian is given by

$$\mathcal{H}_3 = \begin{pmatrix} \omega_0 - i\gamma_{QE}/2 & g_1\sqrt{N/3} & g_M \\ g_1\sqrt{N/3} & \omega_1 - i\gamma_p/2 & 0 \\ g_M & 0 & \omega_M - i\gamma_p/2 \end{pmatrix}, \quad (7)$$

where $g_M = \sqrt{\sum_{l=2}^{\infty} g_l^2}$ and $\omega_M = \sum_{l=2}^{\infty} \omega_l g_l^2 / \sum_{l=2}^{\infty} g_l^2$. Note that the coupling between the collection of QEs and the dipole mode is collectively enhanced by a factor of $\sqrt{N/3}$ (with the factor 3 coming from the threefold degeneracy of the dipole mode). In contrast, there is no collective enhancement of the coupling to the multipoles as each QE interacts with a separate localized pseudomode [see Fig. 4(c)].

From this Hamiltonian, it is also possible to find analytical expressions for the Rabi splitting, Ω_R, between the hybrid modes. In particular, for the case in which $\omega_0 = \omega_1$, we obtain to a good approximation

$$\Omega_R \approx \sqrt{g_1^2 \frac{N}{3} - \frac{1}{4}\left(\frac{\gamma_{QE} - \gamma_p}{2} + i\delta_{eff}\right)^2}, \quad (8)$$

$$\delta_{eff} = \frac{2g_M^2 \delta_M}{\delta_M^2 + (\frac{\gamma_{QE} - \gamma_p}{2})^2}, \quad (9)$$
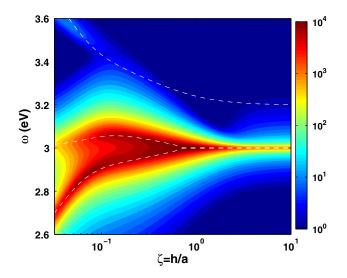

FIG. 5 (color online).   Contour plot: light spectra for $\omega_0 = \omega_1$ and $N = 100$ as calculated from our numerical formalism. Dashed white lines represent the evolution of the three eigenvalues of Eq. 7 as a function of ζ.

with $\delta_M = \omega_M - \omega_1$. This last formula highlights the role of nonradiative modes in the emergence of the collective strong coupling. In the weak coupling regime, nonradiative modes act as an additional decay channel for the QEs whereas in the strong coupling limit, they simply appear as an effective detuning. Figure 5 illustrates the accuracy of the three-level Hamiltonian by showing the light spectrum as a function of ζ and ω for the case of $N = 100$ obtained with our full numerical framework (contour plot) and the eigenvalues analytically calculated from Eq. 7, displayed as dashed white lines.

In conclusion, we have shown how the weak coupling picture of quenching is transformed when the strong coupling regime emerges. While in the weak-coupling limit, the nonradiative EM modes of the nanoparticle act as an effective bath for QE decay, they become a pseudomode that is able to reversibly exchange energy with the QE when entering the strong-coupling regime. This energy transfer occurs between each emitter and a localized pseudomode and is thus noncooperative. However, when the number of QEs increases, collective strong coupling of many QEs with the radiative dipole mode of the nanoparticle builds up, even at very short distances. Simple analytical formulas quantifying individual and collective strong coupling have been derived, and a complete numerical framework reaching far beyond the model system analyzed in this work has been presented. This makes our approach useful for both insightful and quantitative investigations of strong coupling between quantum emitters and localized surface plasmons.

[1] E. Dulkeith, A. C. Morteani, T. Niedereichholz, T. A. Klar, J. Feldmann, S. A. Levi, F. C. J. M. Van Veggel, D. N. Reinhoudt, M. Möller, and D. I. Gittins, Phys. Rev. Lett. **89**, 203002 (2002).

[2] P. Anger, P. Bharadwaj, and L. Novotny, Phys. Rev. Lett. **96**, 113002 (2006).

[3] S. Kühn, U. Håkanson, L. Rogobete, and V. Sandoghdar, Phys. Rev. Lett. **97**, 017402 (2006).

[4] C. M. Galloway, P. G. Etchegoin, and E. C. Le Ru, Phys. Rev. Lett. **103**, 063003 (2009).

[5] P. Bharadwaj, B. Deutsch, and L. Novotny, Adv. Opt. Photonics **1**, 438 (2009).

[6] D. J. Bergman and M. I. Stockman, Phys. Rev. Lett. **90**, 027402 (2003).

[7] M. Noginov, G. Zhu, A. M. Belgrave, R. Bakker, V. M. Shalaev, E. E. Narimanov, S. Stout, E. Herz, T. Suteewong, and U. Wiesner, Nature (London) **460**, 1110 (2009).

[8] K. E. Dorfman, P. K. Jha, D. V. Voronine, P. Genevet, F. Capasso, and M. O. Scully, Phys. Rev. Lett. **111**, 043601 (2013).

[9] A. Akimov, A. Mukherjee, C. Yu, D. Chang, A. Zibrov, P. Hemmer, H. Park, and M. Lukin, Nature (London) **450**, 402 (2007).

[10] J. Bellessa, C. Bonnand, J. C. Plenet, and J. Mugnier, Phys. Rev. Lett. **93**, 036404 (2004).

[11] P. Vasa, R. Pomraenke, S. Schwieger, Y. I. Mazur, V. Kunets, P. Srinivasan, E. Johnson, J. E. Kihm, D. S. Kim, E. Runge, G. Salamo, and C. Lienau, Phys. Rev. Lett. **101**, 116801 (2008).

[12] T. Schwartz, J. A. Hutchison, C. Genet, and T. W. Ebbesen, Phys. Rev. Lett. **106**, 196405 (2011).

[13] A. González-Tudela, P. A. Huidobro, L. Martín-Moreno, C. Tejedor, and F. J. García-Vidal, Phys. Rev. Lett. **110**, 126801 (2013).

[14] A. González-Tudela, P. A. Huidobro, L. Martín-Moreno, C. Tejedor, and F. J. García-Vidal, Phys. Rev. B **89**, 041402 (R) (2014).

[15] A. Trügler and U. Hohenester, Phys. Rev. B **77**, 115403 (2008).

[16] E. Waks and D. Sridharan, Phys. Rev. A **82**, 043845 (2010).

[17] C. V. Vlack, P. T. Kristensen, and S. Hughes, Phys. Rev. B **85**, 075303 (2012).

[18] M. M. Dvoynenko and J.-K. Wang, Opt. Lett. **38**, 760 (2013).

[19] K. V. Nerkararyan and S. I. Bozhevolnyi, Opt. Lett. **39**, 1617 (2014).

[20] S. Savasta, R. Saija, A. Ridolfo, O. Di Stefano, P. Denti, and F. Borghese, ACS Nano **4**, 6369 (2010).

[21] Y. Sugawara, T. A. Kelf, J. J. Baumberg, M. E. Abdelsalam, and P. N. Bartlett, Phys. Rev. Lett. **97**, 266808 (2006).

[22] N. T. Fofang, T.-H. Park, O. Neumann, N. A. Mirin, P. Nordlander, and N. J. Halas, Nano Lett. **8**, 3481 (2008).

[23] A. E. Schlather, N. Large, A. S. Urban, P. Nordlander, and N. J. Halas, Nano Lett. **13**, 3281 (2013).

[24] V. N. Pustovit and T. V. Shahbazyan, Phys. Rev. Lett. **102**, 077401 (2009).

[25] L. Novotny and B. Hecht, *Principles of Nano-optics* (Cambridge University Press, Cambridge, England, 2012).

[26] L.-W. Li, P.-S. Kooi, M.-S. Leong, and T.-S. Yee, IEEE Trans. Microwave Theory Tech. **42**, 2302 (1994).

[27] E. D. Palik, *Handbook of Optical Constants of Solids* (Academic Press, New York, 1998), Vol. 3.

[28] B. Huttner and S. M. Barnett, Phys. Rev. A **46**, 4306 (1992).

[29] H. T. Dung, L. Knöll, and D.-G. Welsch, Phys. Rev. A **57**, 3931 (1998).

[30] M. Wubs, L. G. Suttorp, and A. Lagendijk, Phys. Rev. A **70**, 053823 (2004).

[31] See Supplemental Material at http://link.aps.org/supplemental/10.1103/PhysRevLett.112.253601 for a detailed account of the numerical framework, in which Refs. [32–34] are cited.

[32] H. T. Dung, L. Knöll, and D.-G. Welsch, Phys. Rev. A **62**, 053804 (2000).

[33] C. F. Bohren and D. R. Huffman, *Absorption and Scattering of Light by Small Particles* (John Wiley & Sons, New York, 2008).

[34] P. Yao, C. V. Vlack, A. Reza, M. Patterson, M. M. Dignam, and S. Hughes, Phys. Rev. B **80**, 195106 (2009).